TASK QUARTERLY 6 No 1 (2002), 187–208

UNSTEADY FLOW SIMULATION IN HYDRAULIC MACHINERY

ALBERT RUPRECHT

Institute of Fluid Mechanics and Hydraulic Machinery,
University of Stuttgart,
Pfaffenwaldring 10, D-70550 Stuttgart, Germany
ruprecht@ihs.uni-stuttgart.de

(Received 26 August 2001; revised manuscript received 24 December 2001)

Abstract: In the field of hydraulic machinery Computational Fluid Dynamics (CFD) is routinely used today in research and development as well as in the daily design phase. Today in industry mostly steady-state simulations are applied. In this paper, however, an overview of unsteady simulations is shown for different applications. The presented examples contain problems with self- excited unsteadiness, vortex rope in the draft tube, as well as applications with externally forced unsteadiness by changing or moving geometries, and rotor-stator interactions. For the shown applications the requirements, potential and limitations of unsteady flow analysis are assessed.

Keywords: unsteady RANS, parallel computing, hydro turbine, rotor-stator interaction, vortex rope

1. Introduction

For more than a decade Computational Fluid Dynamics (CFD) is intensively used in the field of hydraulic machinery in research and development as well as in the daily design business. Early successful demonstrations are given *e.g.* in the GAMM workshop [1]. The applications are steadily increasing. This is expressed in Figure 1, showing the percentage of papers dealing with CFD presented at the IAHR

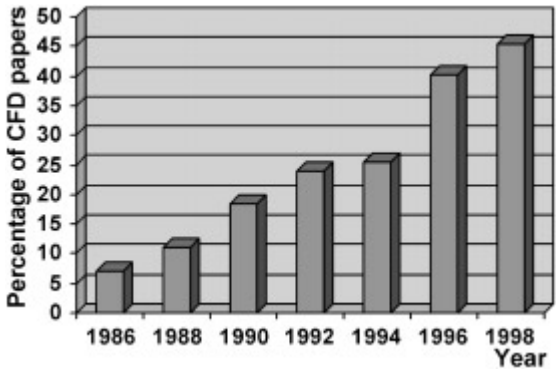

Figure 1. Percentage of papers at the IAHR-Symposium dealing with CFD

Symposium on Hydraulic Machinery and Cavitation, one of the most important conferences in hydraulic machinery. Starting with Q3D-Euler and 3D-Euler today usually simulations based on the Navier-Stokes equations are used.

Nowadays it is fairly standard to simulate the different components separately. By assuming steady-state uniform flow conditions in circumferencial direction only one blade passage of stator and rotor has to be considered. However, since there are strong interactions between the components, especially between guide vanes (stator) and runner, it is necessary to introduce this interaction into the simulation. Many attempts have been made lately to do this by applying an averaging procedure in the circumferential direction. This allows us to consider only one channel of stator and rotor, and to apply a steady-state computation, resulting in a severe saving of computer resources. The obtained results are usually sufficiently accurate compared to measurements and can be applied for turbine design, *e.g.* [2–4].

However, many problems in turbomachinery arise from unsteady flow phenomena. In order to get information on this phenomena or solutions to the problems, unsteady flow analyses are necessary. This requires a much higher computational effort, a factor 10 – 100 compared to the steady-state computations, depending on the problem and on the degree of model simplifications. With today's computers and software, however, unsteady problems can be solved.

Two major groups of unsteady problems can be distinguished:

1. The first group are flows with **externally forced unsteadiness**. This can be caused by unsteady boundary conditions or by changing of the geometry with time. Examples are the closure of a valve, the change of the flow domain in a piston pump, or the rotor-stator interactions, where the geometry of the flow domain changes with the rotation of the runner.
2. The second group are flows with **self-excited unsteadiness**, which are *e.g.* turbulent motion, vortex shedding (Karman vortex street) or unsteady vortex behavior (*e.g.* vortex rope in a draft tube). Here the unsteadiness is obtained without any change of the boundary conditions or of the geometry. There can also occur a combination of both groups (*e.g.* flow induced vibrations, change of geometry caused by vortex shedding). All these phenomena can take place in a turbine or pump and require different solution procedures.

In the field of hydraulic machinery one deals with flows of rather high Reynolds numbers ($10^6 - 10^8$). Therefore the turbulence frequencies are extremely high and can not be resolved by the computational grid and the time steps. Because of that the unsteadiness caused by turbulent motion is not considered here. Here only the unsteadiness of the mean flow is treated. In the following the two examples of unsteadiness are considered:

- part load vortex rope in the draft tube (self-excited unsteadiness)
- stator-rotor interaction (externally forced unsteadiness).

Lets us consider Francis turbines which are mainly installed in huge hydro power stations. In the last four decades the maximum power output of a Francis turbine has reached 800 MW. The peak efficiency reached more than 95%. This improvement has been obtained mostly by detailed measurements in model tests.

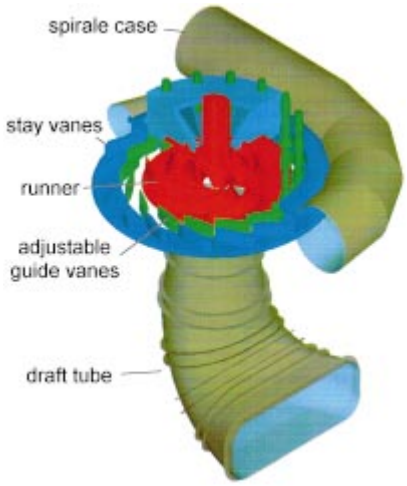

Figure 2. Turbine geometry

In the last decade these measurements are supported by numerical flow calculations. The main components of a Francis turbine are shown in Figure 2.

1.1. Stator-rotor interaction

In order to study the stator-rotor interaction it is necessary to simulate the unsteady flow in the complete turbine. Due to the non-uniform inflow from the spiral case and due to the unequal pitching of guide vanes and runner it is necessary to consider the entire turbine with all channels of the runner and of the tandem cascade (stay vanes and guide vanes). Typically a Francis turbine shows 20 – 24 tandem cascade channels and 9 – 13 runner channels. For an accurate solution each channel has to be resolved with approximately 100 000 nodes. Therefore the unsteady simulation of an entire Francis turbine can only be carried out on high performance computers in parallel.

1.2. Draft tube vortex rope

One of the most difficult problems in the operation of hydro power plants (especially with Francis turbines) is the appearance of a vortex rope in the draft tube under part load conditions. The rotation of the vortex rope – it usually rotates with 20 – 40% of the turbine speed – causes severe rotating pressure fluctuations. In addition to these rotating pressure fluctuations in bended draft tubes (elbow draft tubes) under certain conditions also a synchronous component of the pressure surge can be observed. This synchronous fluctuation acts as an excitation which can introduce discharge and pressure oscillations in the water system. As a consequence the entire power plant can show severe oscillation, this can lead to restrictions of the range of operation.

2. Basic equations

In hydraulic turbomachinery today usually the Reynolds averaged Navier-Stokes equations for an incompressible flow are applied:

$$\frac{\partial U_i}{\partial t} + U_j \frac{\partial U_i}{\partial x_j} + \frac{1}{\rho}\frac{\partial P}{\partial x_i} - \frac{\partial}{\partial x_j}\left(v\left(\frac{\partial U_i}{\partial x_j} + \frac{\partial U_j}{\partial x_i}\right) - \tau'_{ij}\right) = 0 \tag{1}$$

τ'_{ij} are the Reynolds stresses, which are calculated from the turbulence model. The continuity equation for incompressible flow reads

$$\frac{\partial U_i}{\partial x_i} = 0 \tag{2}$$

and does not contain a time depending term.

The above description of the flow in the Eulerian coordinates can be applied for unsteady boundary condition problems as well as for self-excited unsteadiness. However, to express problems with moving geometries in Eulerian coordinates is more difficult. At the moving boundary a Lagrangian description can be applied very easily since the fluid particles can be traced by this method. Combining these two methods an Arbitrary Lagrangian Eulerian (ALE) method can be utilized. This method is suitable for the solution of problems with moving boundaries. In the ALE method the reference coordinates can be chosen arbitrary. In this referential coordinate system the material derivative can be described as

$$\frac{\partial f(x_i^L,t)}{\partial t} = \frac{\partial f(x_i^R,t)}{\partial t} + (u_j - w_j)\frac{\partial f(x_i^E,t)}{\partial x_j}, \tag{3}$$

where x_i^L – Lagrangian coordinates, x_i^R – referential coordinates, x_i^E – Eulerian coordinates, W_i – reference velocity.

The momentum equations in the ALE formulation can be written as follows:

$$\frac{\partial U_i}{\partial t} + (U_j - W_j)\frac{\partial U_i}{\partial x_j} + \frac{1}{\rho}\frac{\partial P}{\partial x_i} - \frac{\partial}{\partial x_j}\left(v\left(\frac{\partial U_i}{\partial x_j} + \frac{\partial U_j}{\partial x_i}\right) - \tilde{\tau}_{ij}\right) = 0. \tag{4}$$

The moving of the reference system W_i can be chosen arbitrary. If W_i is equal to zero one gets the Eulerian description, on the other hand, if W_i is equal to the velocity of the fluid particle the Lagrangian formulation is obtained. The convective term in the transport equations for scalar quantities changes in the same way as in the momentum equations. This applies also to the turbulence equations.

For industrial applications today mostly the k-ε turbulence model is used. This model, however, is not suitable for unsteady problems. It does not distinguish between the resolved unsteady vortex structure and the averaged turbulence. Improved results can be obtained by applying multi-scale models, which take into account the different vortex scales. Also other approaches like filtering techniques, *e.g.* [5] are successfully applied. Especially for problems with self-excited unsteadiness an improved turbulence model is essential.

3. Numerical procedures

The analyses are performed using the finite element code FENFLOSS developed at the University of Stuttgart. FENFLOSS is based on the Reynolds averaged Navier-Stokes equations with different models of turbulence. It uses a segregated solution algorithm, where the three momentum equations are solved separately. The pressure is calculated by a pressure correction algorithm. The time discretisation is obtained by a fully implicit 3-level scheme of 2$^{\text{nd}}$ order. The spatial discretisation is done by using bi-linear 8-node brick elements. For the solution of the linear equation systems a conjugated gradient method is used for non-symmetrical matrices (BICGSTAB2) [6] with an ILU-preconditioning. The flow in all components except the runner is

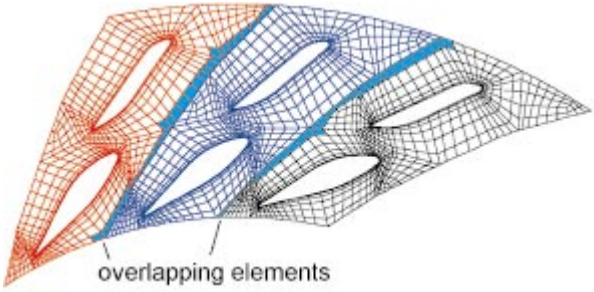

Figure 3. Overlapping grid for parallel computation

described in a fixed frame of reference, whereas the flow in the runner is expressed in a co-ordinate system rotating with the runner.

The flow in the different components is calculated in parallel by using domain decomposition with matching overlapping meshes. This is shown schematically in Figure 3 for the tandem cascade. The data exchange is carried out in the BICGSTAB2 solver. To obtain the grid partitioning METIS [7] and JOSTLE [8] are applied.

The numerical realization of moving or changing grids can either be obtained by deformation of an existing mesh in each time step. For large deformations this requires an automatic grid smoothing algorithm or even an automatic remeshing after a few time steps. Another method is the use of different embedded grids, which can move against each other. In this case a sliding interface between the non-matching grids is required. Here the second method is applied.

At the interfaces between the components non-matching overlapping grids are used. One difficulty results from the movement of the runner geometry against the guide vanes and the draft tube. Because of that the data exchange between the different calculation domains (processors) varies from time step to time step. The information exchange from one component to the other is organised in the form of dynamical boundary conditions. The exchange is made by interpolation of the node values in the downstream direction and prescribing the fluxes in the upstream direction. The data are exchanged in each iteration. The grids for the different components are overlapping and non-matching, as schematically shown in Figure 4.

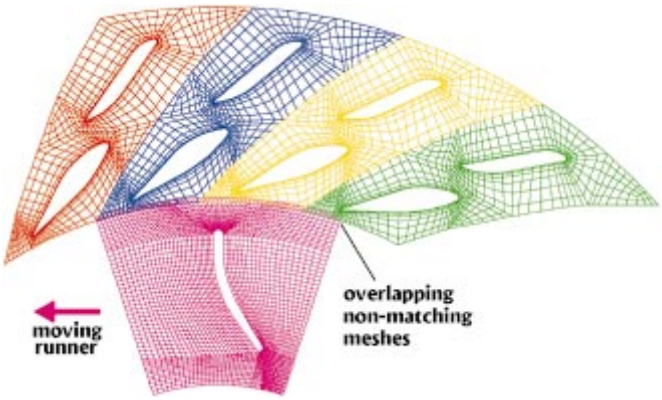

Figure 4. Sliding interface, overlapping non-matching grids

At the interface stator-rotor and rotor-draft tube for each time step the locations of the runner nodes have to be evaluated and the velocity data have to be transformed from the fixed to the rotating frame of reference. A flow chart of the solution process is shown in Figure 5. Details of the algorithm are described in [9, 10].

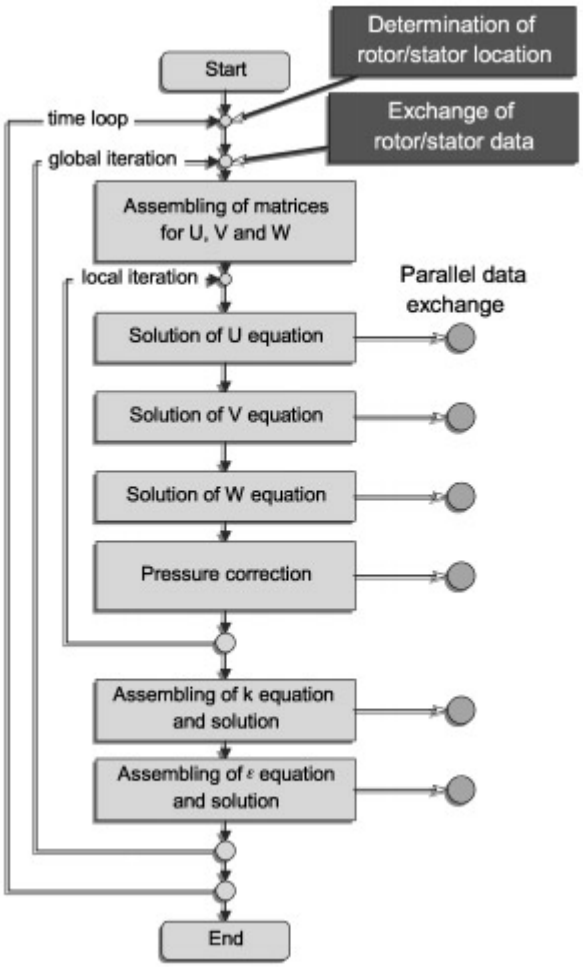

Figure 5. Flow chart of FENFLOSS

3.1. Computer

The calculations are carried out on different parallel machines, among them a CRAY T3E machine with 512 processors, 128 MB RAM per processor and a peak performance of 412 Gflops. The data exchange is implemented using MPI-routines.

3.2. Speed-up

In order to show the performance, a steady-state calculation of a draft tube with 1 000 000 elements is considered. For the speed-up the simulation on 32 processors is used as reference. This is the smallest partitioning on which the simulation can be carried out on Cray T3E/512. The partitioning on 32 processors is shown in Figure 6.

The speed-up for 64, 128 and 256 processor is presented in Figure 7. The highest possible values are a measure of the parallel overhead caused by the overlapping elements. It can be seen that the efficiency of the program increases nearly according to the highest possible values.

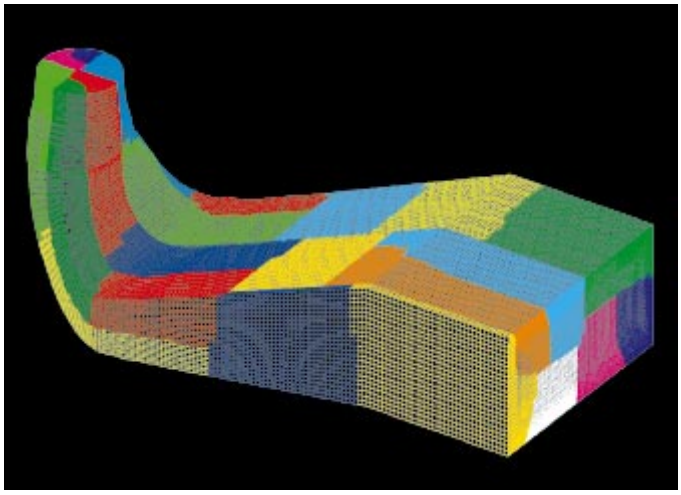

Figure 6. Partitioning of a draft tube

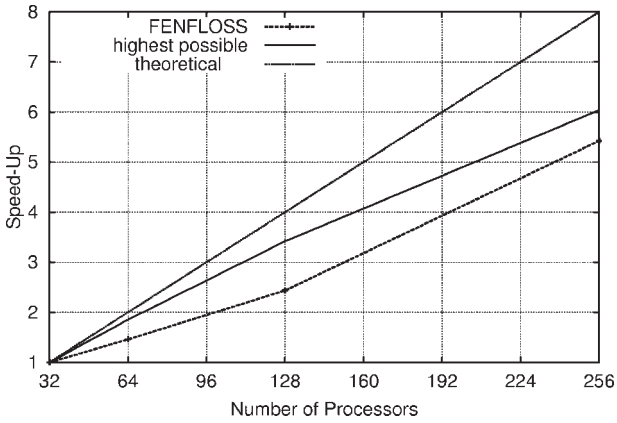

Figure 7. Speed-up for draft tube example

3.3. Postprocessing

The complex unsteady simulation leads to an enormous amount of data, which have to be processed and visualised. This requires a powerful graphics machine and a sophisticated software. The software used is COVISE developed at the University Computer Center (RUS), which allows the visualization in Virtual Reality. At RUS a CUBE with 4 projection walls is installed. The computer hardware is a Silicon Graphics Onyx2 double rack system with 14 R10000 CPUs and 4 GB of main memory. The Onyx2 has three InfiniteReality pipes each equipped with two raster managers. An investigation of the turbine in the VR-Cube is shown in Figure 8.

Figure 8. Investigation in VR

4. Applications

4.1. Vortex rope

4.1.1. Vortex rope in a straight diffuser

As an example of self-excited unsteady flow, the simulation of a vortex rope in a draft tube is shown. At first a straight axisymmetrical diffuser is investigated. Here the different behavior of the above mentioned turbulence models is demonstrated. The inflow conditions to the diffuser are chosen according to the part load operation of a Francis turbine. This means that the flow shows a strong swirl component. The inlet velocity distribution, taken from [11] and the geometry are presented in Figure 9.

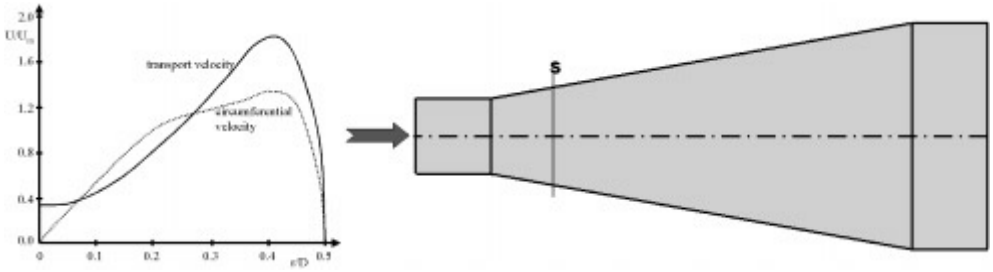

Figure 9. Geometry and inlet conditions

Applying the standard k-ε model the unsteady simulation leads to steady-state flow conditions. In Figure 10 the velocity vectors in the symmetry plane and in 3 cross-sections are shown. It can be observed that in the center of the diffuser inlet a strong recirculation region is obtained. This region, however, is steady-state and symmetrical.

Applying the extended k-ε model the flow becomes unsteady. The instantaneous flow condition for a certain time step is given in Figure 11, where an iso-pressure surface as well as the secondary velocity vectors in three cross-sections are plotted. Clearly the cork-screw type flow with an unsymmetrical form is visible, although the geometry and the boundary conditions are completely axisymmetrical.

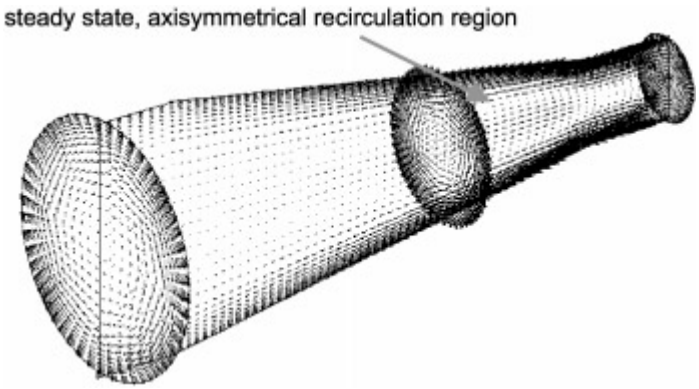

Figure 10. Velocity vectors, standard k-ε model

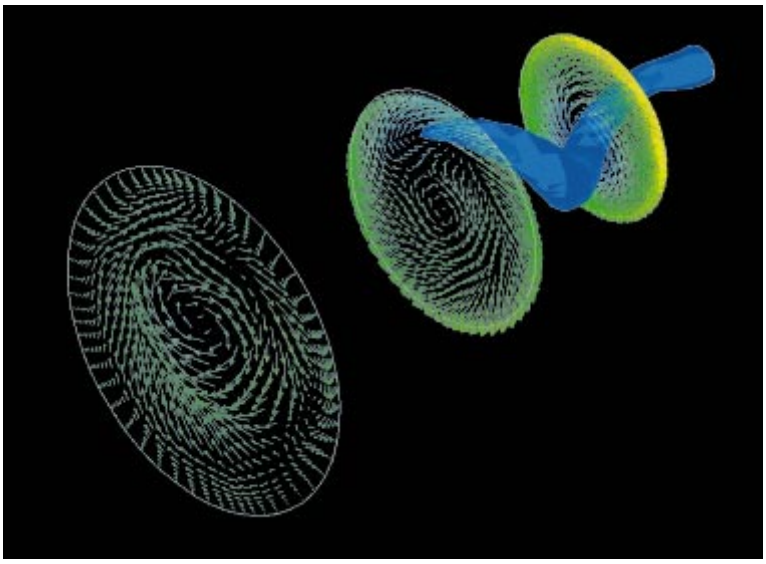

Figure 11. Iso-pressure surface and secondary flow in a vortex rope

In Figure 12 the secondary velocity and the low pressure region, which represents the vortex center, are shown in the cross-section S, indicated in Figure 9, for four different time steps. Clearly the revolution of the vortex center can be observed. This, of course, causes pressure fluctuations and therefore dynamical forces on the draft tube surface.

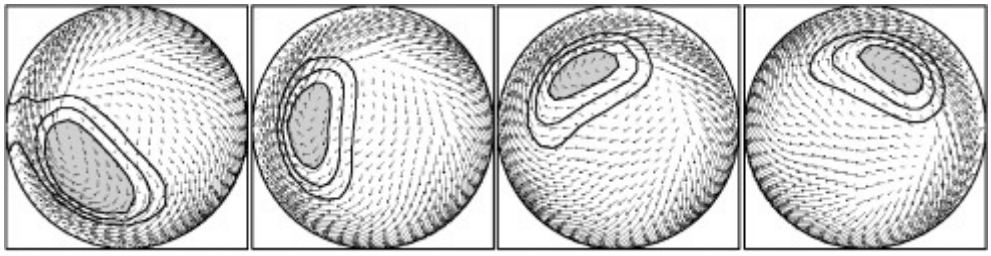

Figure 12. Secondary motion and low pressure region for different time steps

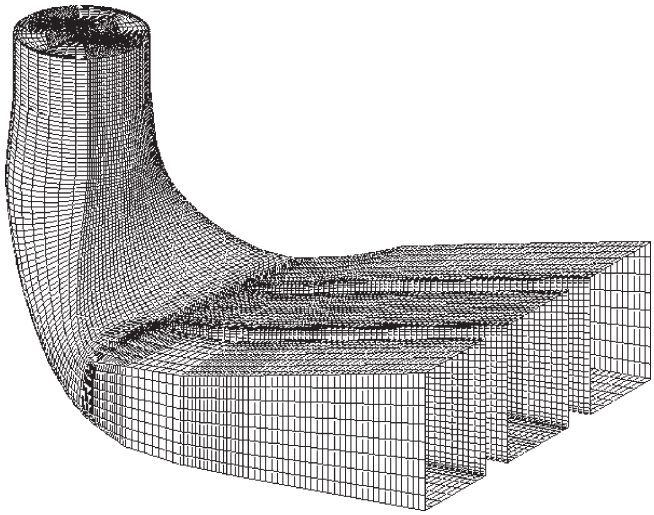

Figure 13. Grid of the draft tube

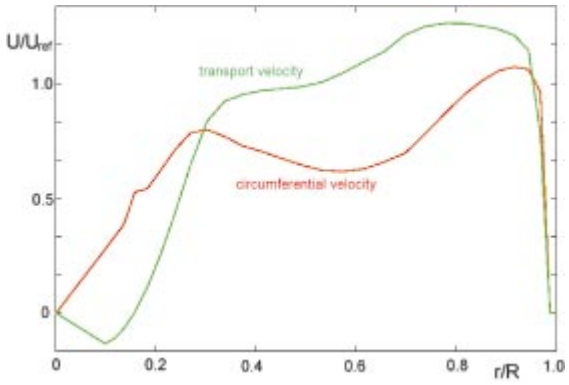

Figure 14. Velocity distribution at the inlet

As already mentioned the application of the standard k-ε model leads to a steady-state symmetrical solution. This is also reported in [11]. Applying a more sophisticated model, suitable for unsteady flows, one obtains a much lower eddy viscosity than the standard model and, as a consequence, an unsteady vortex movement.

4.1.2. Vortex rope in an elbow draft tube

The draft tube shape of hydraulic machinery is usually more complicated. The investigated elbow draft tube consists of three outflow channels with two piers in between. At the inlet the computational domain is enlarged up to the runner hub. The area between the runner hub and inlet of the draft tube is simplified with a straight tube. The computational grid is shown in Figure 13. It consists of about 250 000 nodes.

A circumferential averaged velocity profile obtained from a 3-dimensional steady-state runner calculation under part load conditions is taken as the inlet condition for the calculation domain, Figure 14. At the outlet a constant pressure value is assumed.

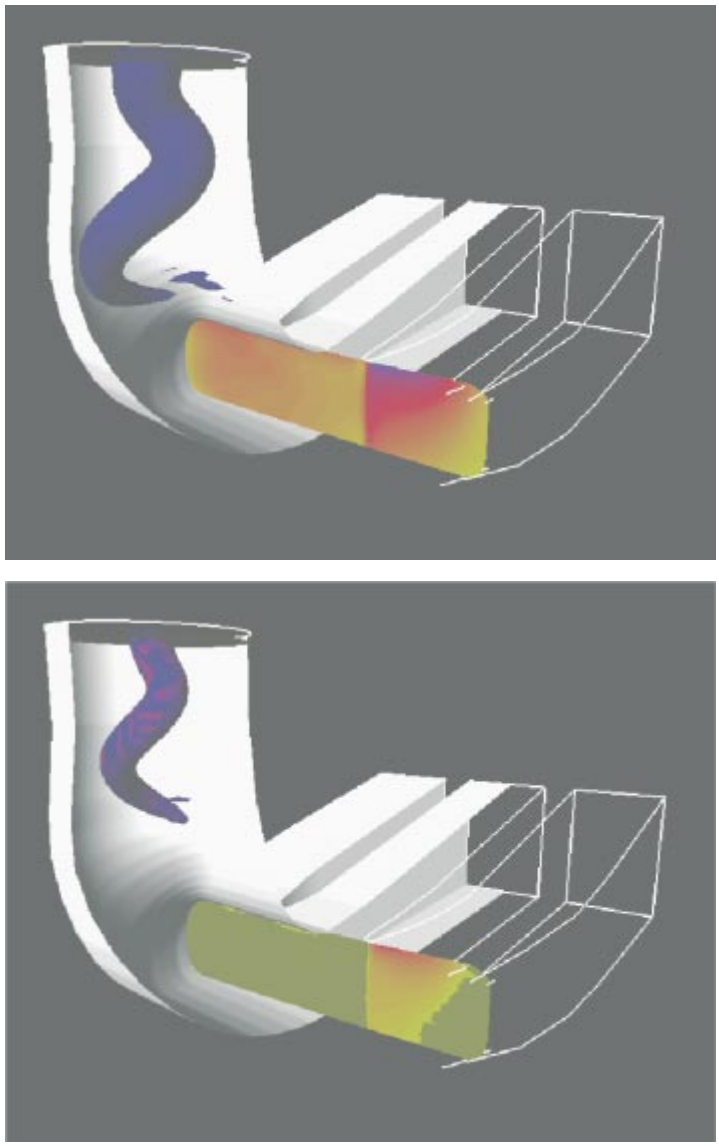

Figure 15. Vortex rope in the draft tube for two time steps

The results show a strongly unsteady flow behaviour in the draft tube. Figure 15 presents the vortex rope as an iso-surface of the pressure for two different time steps. It can be detected that the vortex rope has the shape of a rotating cork-screw. The changing size of the vortex rope indicates strong pressure surges, which means a synchronous, non-rotating pressure fluctuation. This synchronous part usually causes the problems.

In order to compare the unsteady flow simulation with measurements, the pressure values are taken in each time step at the same position, where the pressure transducers are located in the experiment (Figure 16). Exemplary in Figure 17 and 18, the measured and calculated pressure over time is shown for the position 3 and 4.

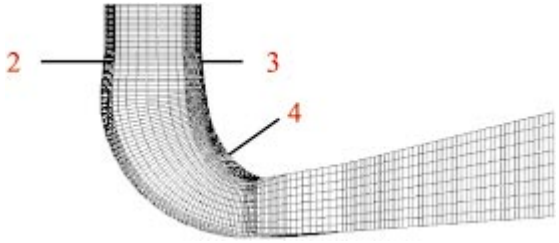

Figure 16. Location of the pressure measurement at the draft tube

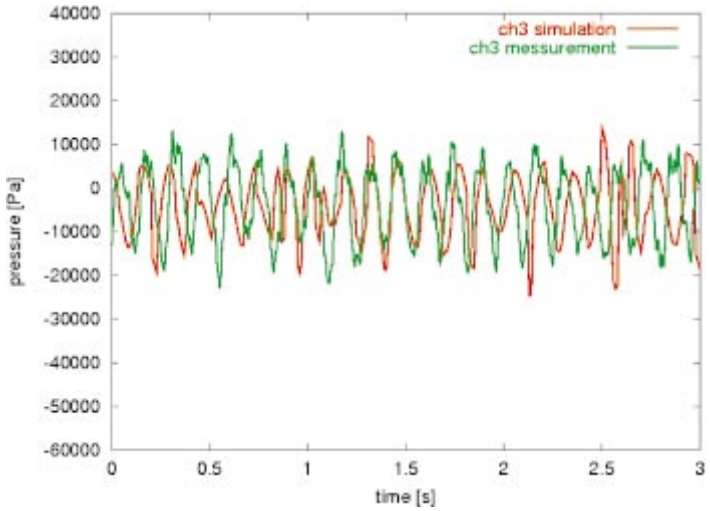

Figure 17. Pressure at position 3, comparison of measurement and simulation

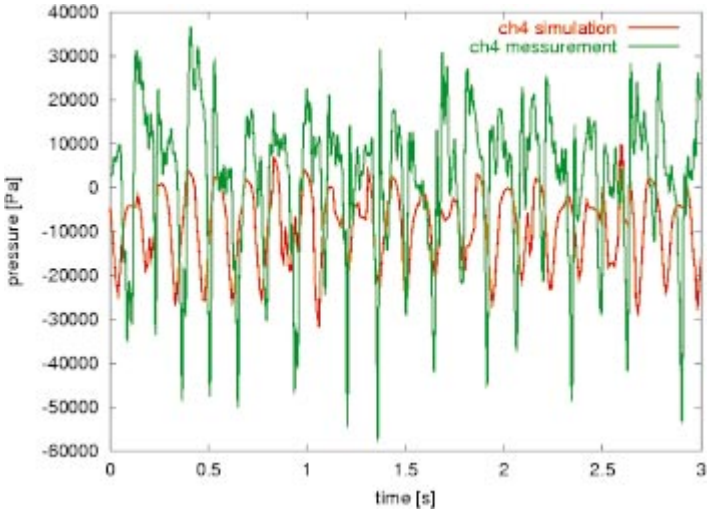

Figure 18. Pressure at position 4, comparison of measurement and simulation

It can clearly be seen that the simulated pressure at position 3 agrees quite well with the measured values. The amplitude of the pressure oscillation is predicted a little too low. The frequency however agrees extremely well.

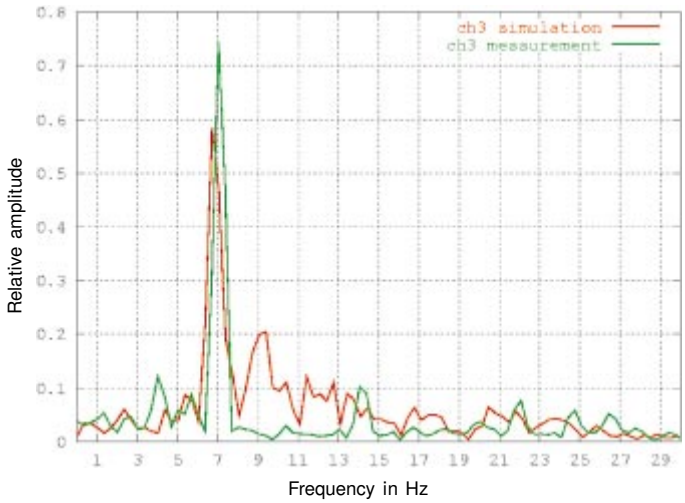

Figure 19. Fast Fourier Transformation for the point 3

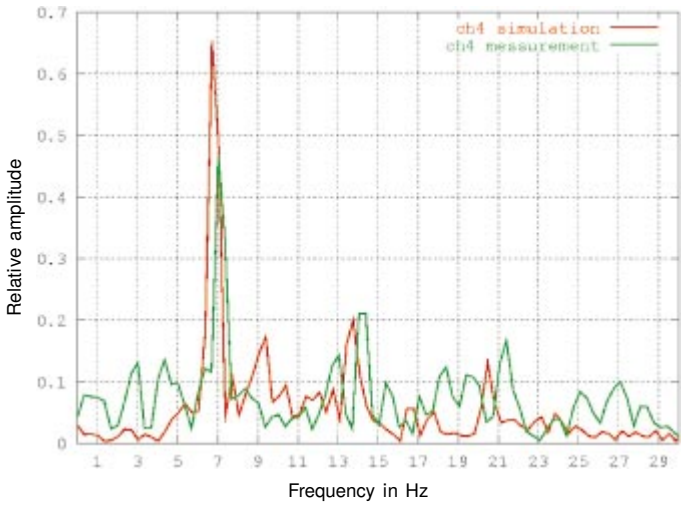

Figure 20. Fast Fourier Transformation for the point 4

For position 4 the frequency of the measured and calculated pressure also agrees quite well. The amplitudes, however, show a greater discrepancy. As would be expected, the amplitude of the calculation in channel 4 is much more damped compared to the measurement. Possible reasons are the fixed discharge in calculation, caused by the steady inlet condition at the draft tube, and the damping effects to the swirl by the turbulence model.

A Fast Fourier Transformation is also carried out for the measured and calculated signals of position 3 and 4. In Figure 19 and 20 the relative amplitude of the signal is shown over the frequency range. In both cases one can detect the frequency of 7 Hz, that is the frequency of the vortex rope.

The presented results are obtained on Hitachi SR 2201 using 16 processors. The simulation of one point of operation takes $\sim$10 hours depending on the point of operation.

4.1.3. Discussion

The application of the standard k-ε model for the straight diffuser as well as for the elbow draft tube leads to a steady-state symmetrical solution. The results shown above are achieved by applying the multi-scale k-ε model of Kim [12] together with a streamline curvature correction. This model shows a much lower eddy viscosity than the standard model, especially in swirling flows. The application of wall functions does not give any problems here, since the flow instability has its origin in the center and is not affected by the prediction of the near-wall region.

4.2. Stator-rotor interaction

4.2.1. Francis turbine

As a first example for the calculation of stator-rotor interaction a Francis turbine is shown. In this case the entire turbine from spiral casing to the draft tube is considered. The computational grid of the investigated turbine is shown in Figure 20. The different colours mark the different processors. The simulation is carried out on different grids. In Figure 21 a rather coarse grid (approximately 2 million nodes) is shown for which a decomposition into 96 domains (processors) is done. In more detail, the grids in the tandem cascade (stay vanes and guide vanes) are also shown.

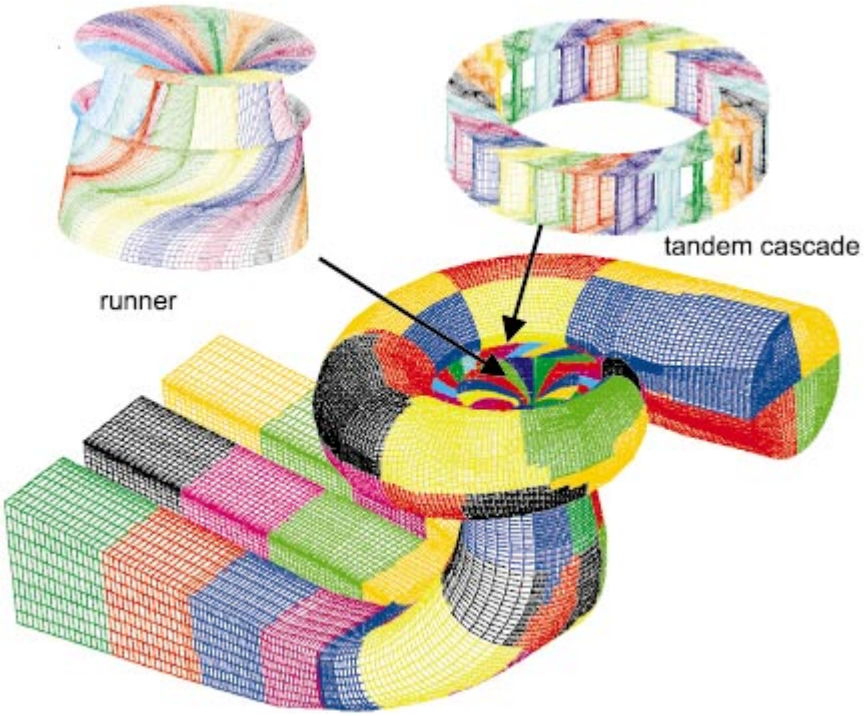

Figure 21. Computational grid of the entire Francis turbine

The boundary conditions for the simulation are a fully developed pipe flow at the inlet to the spiral case and a free outflow condition at the draft tube outlet. The guide vanes and the runner speed are adjusted to the turbine optimum. The time

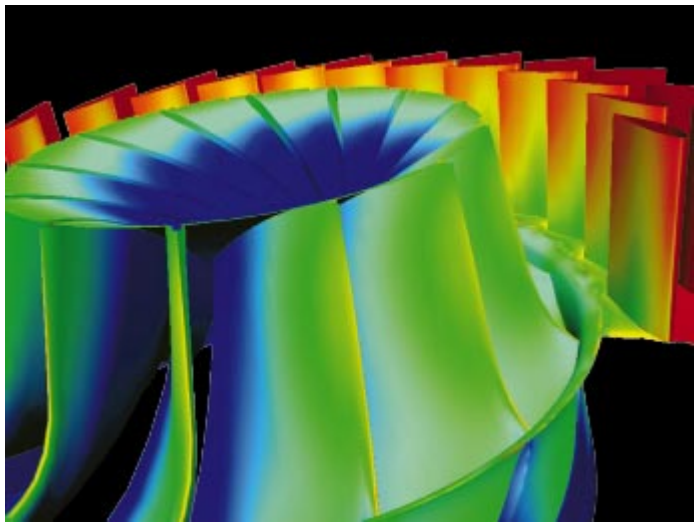

Figure 22. Pressure distribution for a certain time step

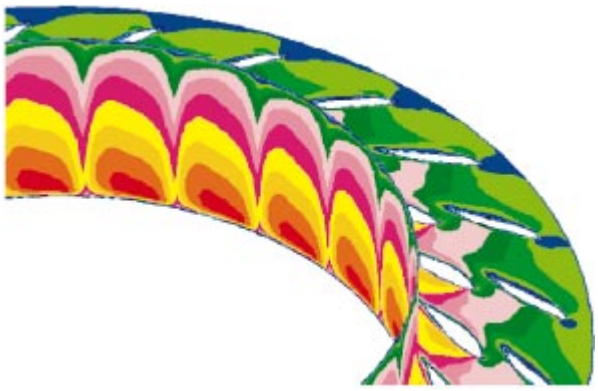

Figure 23. Velocity distribution in the tandem cascade

step for the calculation has been chosen according to the rotation of the runner by 1 degree.

As already mentioned the processing of the results of the unsteady simulation requires a great effort. Here only some of the results are shown exemplarily. In Figure 22 the pressure distribution at a certain time step is shown. One can see the high pressure in the stay vanes. The pressure decreases because of the flow acceleration. At the runner inlet, clearly a stagnation region can be observed. Also a non-uniform pressure distribution over the height of the stay vanes and the runner inlet can be noticed. This is caused by an acceleration of the flow due to the turning from the horizontal to the vertical direction. This acceleration can also be seen in Figure 23, where the velocity distribution in a circumferential plane and in the mid plane of the tandem cascade (stay and guide vanes) is plotted. Clearly, the wakes of the blades and the non-uniform distribution across the height can be observed.

The simulation leads to the unsteady pressure distribution especially on the guide vanes and on the runner blades. From this results the dynamic forces can be

evaluated. By applying a structural analysis also the dynamic stresses can be obtained. This can lead to a safer design, which would not be possible without super-computers. For more details the reader is referred to [13].

4.2.2. Axial turbine

In a second example the stator-rotor interaction is shown for an axial turbine. Since for this geometry detailed measurements are available, the computational results can be compared with experimental data.

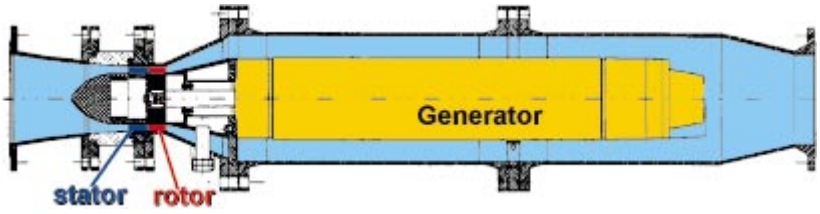

Figure 24. Geometry of the investigated axial turbine

Figure 25. Geometry of rotor and stator

The speciality of this turbine is its relatively low specific speed. It has been designed for pressure recuperation in piping systems. The advantage is that the discharge is nearly independent of the speed. Because of that, the turbine cannot introduce waterhammers in the system. The geometry of the turbine is shown in Figure 24. It consists of the inlet confuser, 12 fixed guide vanes, 15 runner blades and the draft tube. The stator and rotor part is shown in more detail in Figure 25. For the simulation the complete turbine is considered including all flow channels in the guide vanes and in the runner, although a symmetry condition of 120°could be used. The reason is that also a variant with unsymmetrical outlet – a bended draft tube – has been investigated.

The computational mesh consists of more than 2 million grid nodes, part of the grid is shown in Figure 26. These are roughly 60 000 nodes per flow channel. It is a rather coarse grid, considering that the clearance between the runner blades and casing has to be included in the model, which is necessary since the clearance flow very much affects the channel flow because of the short runner blades. The calculations are carried out using the standard k-ε model.

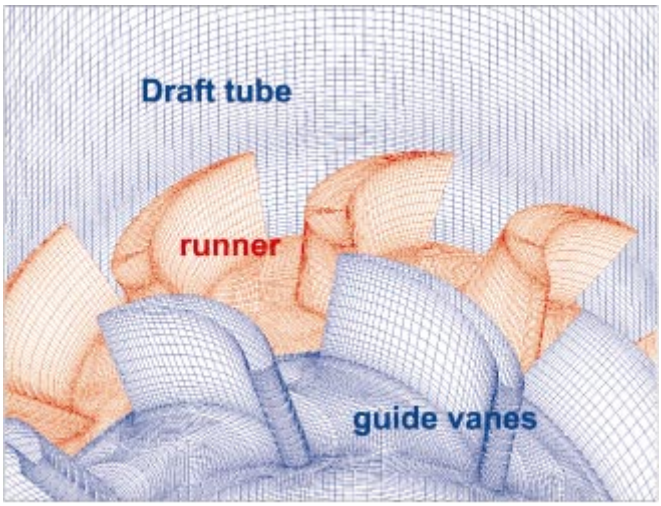

Figure 26. Part of the computational mesh

In the following some results of the calculation will be shown. In Figure 27 the instantaneous flow in the runner is presented. The figure shows the pressure distribution of the runner surface as well as streamlines started at different locations. Looking at the pressure one clearly sees the stagnation point at the leading edge. The location of the stagnation point varies slightly with the runner position. Generally the inlet flow angle seems to be slightly too flat. Therefore the stagnation point is shifted towards the suction side.

Considering the flow in the tip clearance one can observe that at the inlet the shear forces dominate. The flow tends to go from the suction to the pressure side. In the second half of the blade the pressure forces dominate. The flow in the clearance goes from the pressure to the suction side.

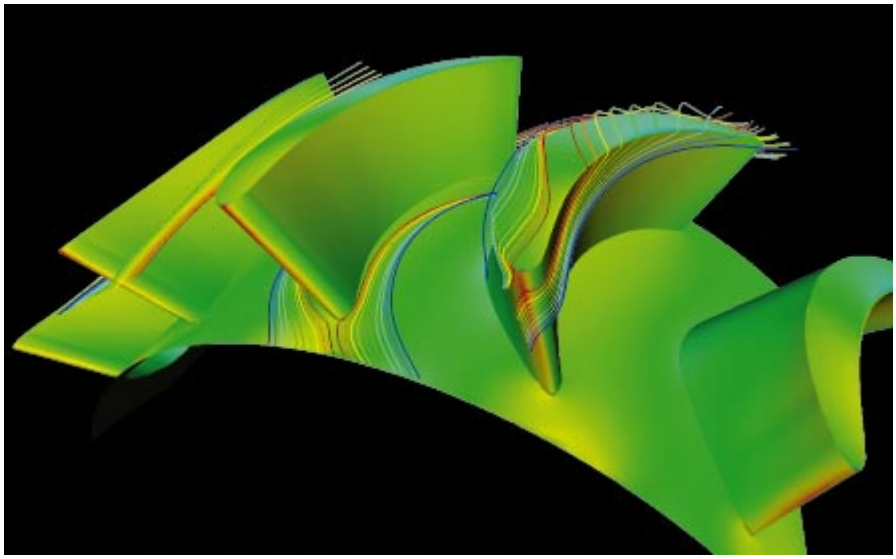

Figure 27. Instantaneous flow in the runner

It can already be seen from these results that the design of the runner is not optimal. This is a first version, in the meantime a much better runner has been designed. However this geometry is numerically investigated since extensive measurements have been carried out for this configuration and the numerical results can be validated.

Figure 28. Calculated pressure distribution for a certain runner position

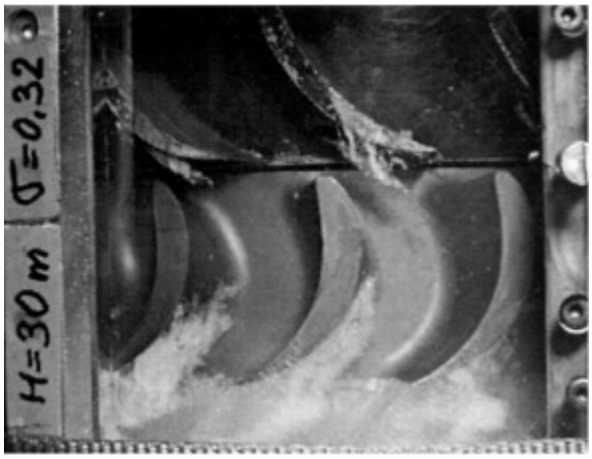

Figure 29. Cavitation observation in the runner

In Figure 28 again the instantaneous pressure for a certain time step is shown. One can observe the low pressure region on the suction side at the top of the runner blades. Clearly visible is the variation of the pressure with the position. The low pressure region corresponds quite well to the cavitation observation at the test rig, see Figure 29. There, one can also observe the variation of the cavitation bubbles according to the runner position.

As a quantitative comparison the pressure at two locations is shown in Figure 30. Position 1 is located in front of the guide vanes and the second position is

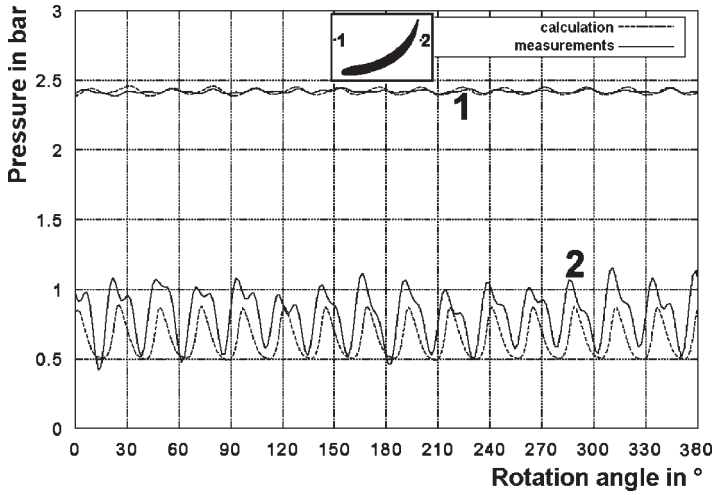

Figure 30. Pressure distribution at two spot points

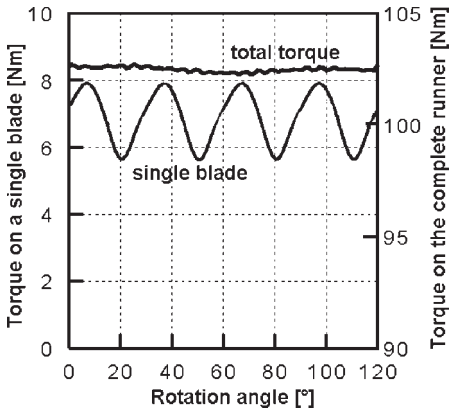

Figure 31. Torque on the runner blades

between the guide vanes and the runner. At both locations the measured and the calculated pressure agree quite well. One can see that even in front of the guide vanes pressure fluctuations can be observed. Between the stator and the rotor, fluctuations of nearly 25% of the turbine head can be seen. This, of course, leads to dynamical forces on the blades. In Figure 31 the torque on one runner blade as well as the torque of the complete runner is shown. The calculated torque fluctuations on a single blade are nearly 30% of the average torque. This is a dynamical force on the blading. The total torque, however, is nearly constant due to the great number of blades and due to different phases of the fluctuations. Further details concerning the turbine and the measurements are published in [14], details on the calculations are given in [15].

4.2.3. Discussion

Since the unsteadiness of the flow is forced by the changing of the geometry, this problem is easier to attack than the examples shown above. The accuracy of the solution depends nearly on the same criteria as for steady-state flow simulations.

The most dominant parameters are grid size, turbulence model, wall distance *etc.*, similar to steady-state problems. Choosing adequate parameters for the steady-state will usually also lead to unsteady solutions of comparable accuracy. As seen in the comparison with the measurements the prediction of pressure (but also of velocities which are not shown here, see [15]) is quite accurate. Therefore this kind of calculation is suitable to predict dynamical forces.

5. Potential, limitations, required resources

The applications show that many unsteady problems in hydraulic machinery can be investigated by CFD and many phenomena can be studied, even rather complicated ones. Here we will discuss again the potential and the limitations as well as the required resources, which are necessary for an unsteady simulation.

Firstly the rotor-stator problem is discussed. It can be said that for this type of flow the unsteady computations behave similar to steady-state computations. The accuracy principally depends on the grid size, on the turbulence model *etc.* used as for the steady-state. Inaccurate unsteady results are usually obtained for similar flow situations as known from steady-state calculations, *e.g.* wake flows, swirling flows *etc.*

It has to be pointed out that the requirements of computational efforts for unsteady flows are much higher than those for the steady-state. Looking at a single component an unsteady simulation needs at least 5 times more computing time. But due to the absence of any periodicity the complete turbine including all stator and rotor channels have to be considered, in opposition to the steady-state, where periodicity can be applied by circumferential averaging. Depending on the type of machine and on the number of guide vanes and runner blades the necessary grid nodes can be increased by a factor of $20-30$, to achieve a similar accuracy. Consequently the computational resources increase by a factor of 100 or more.

Another problem for unsteady computations of a complete turbine or pump is that the flow contains a large range of frequencies. In order to resolve the high frequencies accurately enough a small computational step has to be chosen. This, however, results in very long computational times when also low frequency phenomena have to be resolved.

Concerning the self-excited vortex flow, qualitative predictions can be obtained. Even if the detailed flow behavior may not be kept completely correct (see the amplitudes of the pressure fluctuations) the frequencies and amplitudes of integral quantities (*e.g.* forces) can be predicted with sufficient accuracy for most of the problems. Flow instabilities and correct vortex movements, however, depend very much on the detailed flow situation. Even small changes of velocity can have a great response in the flow structure. There, the vortex instability strongly depends on the swirling rate. Therefore, it is essential to predict the highly swirling flow very accurately, but that is a severe problem for all the turbulence models used in practice today. It is necessary to apply a model, which can handle swirling flow accurately, *e.g.* non-linear models or Reynolds-stress models, since swirling flows are dominated by anisotropic effects. Maybe, sufficiently accurate results can only be achieved by Large Eddy Simulations.

Because the vortices are often very concentrated and consequently show very steep gradients, their prediction requires very fine computational grids. If the vortices move with time a self-adaptive mesh refinement would be desirable. This, however, is rather complicated. Since the required computational effort is very high, parallel computing must be applied in order to obtain reasonable response times. An adaptive grid generation then leads to a dynamical load distribution.

6. Conclusions

Unsteady simulations in hydraulic machinery for different applications have been shown, for self-excited unsteadiness (vortex rope) as well as for externally forced unsteadiness (rotor-stator interactions). All simulations have in common a large requirement of computational resources. Especially for rotor-stator interactions the complete turbine has to be considered and all flow channels in the stator as well as in the rotor have to be included. This leads to many grid nodes and an enormous computational effort.

On the other hand the flow with vortex instability, *e.g.* vortex rope in a draft tube, represents a great challenge for an unsteady simulation. There, the swirl intensity very much affects the overall movement of the vortex. But just strong swirling flows are extremely difficult to calculate and the turbulence models applied today cannot capture this behavior accurately. For this type of flow it is necessary to use improved models of turbulence.

Even if there are problems with the computational accuracy, much information can be obtained from unsteady simulations. For example the dynamical forces in the axial turbine could be predicted with sufficient accuracy in order to allow an assessment of the durability. On the other side flow phenomena can be predicted and a potential to control them can be assessed.

References

[1] *Proc. GAMM-Workshop on 3D Computation of Incompressible Internal Flows*, 1989, Lausanne, Switzerland
[2] Ridelbauch S, Klemm D and Hauff C 1996 *Proc. 18th IAHR Symposium Hydraulic Machinery and Cavitation*, Valencia, Spain, pp. 238–247
[3] Labrecque Y, Sabourin M, Deschênes C 1996 *Proc. Conf. Modelling, Testing and Monitoring for Hydro Powerplants*, Lausanne, Switzerland, pp. 77–86
[4] Sick M, Casey M V and Galphin P F 1996 *Proc. 18th IAHR Symposium Hydraulic Machinery and Cavitation*, Valencia, Spain, pp. 257–266
[5] Magnato F and Gabi M 2000 *Proc. ISROMAC*, Honolulu, USA, vol. **8**
[6] Van der Vorst H A 1994 *Proc. Conf. High Performance Computing and Networking*, München, Germany, pp. 174–183
[7] Schloegel K, Karypis G and Kumar V 1997 *J. Parallel and Distributed Computing* **47** 109
[8] Walshaw C 1999 *Parallel Jostle Library Interface* version 1.1.5, School of Computing and Mathematical Science, University of Greenwich, London
[9] Heitele M, Helmrich T, Maihöfer M and Ruprecht A 1999 *Proc. 5th European SGI/CRAY MPP Workshop*, Bologna, Italy, http://www.cineca.it/mpp-workshop/fullpapers/aruprecht/
[10] Ruprecht A, Bauer C, Gentner C and Lein G 1999 *ASME PVP* **397-2** 173
[11] Skotak A 1999 *Proc. IAHR WG The Behaviour of Hydraulic Machinery under Steady Oscillatory Conditions*, Brno, Czech Rep., paper D.4
[12] Kim S-W and Chen C-P 1989 *Numerical Heat Transfer, Part B* **16** 193

[13] Ruprecht A, Heitele M, Helmrich T, Moser W and Aschenbrenner T 2000 *Proc. 20th IAHR Symposium on Hydraulic Machinery and Cavitation*, Charlotte, USA, paper CFD-S03
[14] Gentner Ch 2000 *Experimentelle und numerische Untersuchung der instationären Strömung in einer Axialturbine*, PhD Thesis, Universität Stuttgart
[15] Bauer C 2001 *Instationäre Berechnung einer hydraulischen Axialturbine unter Berücksichtigung der Interaktion zwischen Leit- und Laufrad*, PhD Thesis, Universität Stuttgart